

# PSGAN: A Generative Adversarial Network for Remote Sensing Image Pan-sharpening

Qingjie Liu, *Member, IEEE*, Huanyu Zhou, Qizhi Xu, Xiangyu Liu, and Yunhong Wang, *Fellow, IEEE*

**Abstract**—Remote sensing image fusion (also known as pan-sharpening) aims to generate a high resolution multi-spectral image from inputs of a high spatial resolution single band panchromatic (PAN) image and a low spatial resolution multi-spectral (MS) image. In this paper, we propose PSGAN, a generative adversarial network (GAN) for remote sensing image pan-sharpening. To the best of our knowledge, this is the first attempt at producing high quality pan-sharpened images with GANs. The PSGAN consists of two parts. Firstly, a two-stream fusion architecture is designed to generate the desired high resolution multi-spectral images, then a fully convolutional network serving as a discriminator is applied to distinct “real” or “pan-sharpened” MS images. Experiments on images acquired by Quickbird and GaoFen-1 satellites demonstrate that the proposed PSGAN can fuse PAN and MS images effectively and significantly improve the results over the state of the art traditional and CNN based pan-sharpening methods<sup>1</sup>.

**Index Terms**—Image fusion, pan-sharpening, GAN, deep learning, remote sensing

## I. INTRODUCTION

RECENTLY, a lot of high resolution (HR) optical Earth observation satellites, such as QuickBird, GeoEye, WorldView-2, and GaoFen-2 have been launched, providing researchers in remote sensing community a large amount of data available for various research fields, such as agriculture [1], land surveying [2], environmental monitoring [3], and so on. To obtain better results, many of these applications require images at the highest resolution both in spatial and spectral domains. However, due to technical limitations [4], satellites usually carry two kinds of optical imaging sensors and acquire images at two different yet complementary modalities: one is a high resolution panchromatic (PAN) image and another one is a low resolution (LR) multi-spectral (MS) image. Pan-sharpening (i.e. panchromatic and multi-spectral image fusion), which aims at generating high spatial resolution MS images by combining spatial and spectral information of PAN and MS images, offers us a good solution to alleviate this problem.

Pan-sharpening could be beneficial for many practical applications, such as change detection, land cover classification,

so it has gained increasing attention within the remote sensing community. Many research efforts have been devoted to developing pan-sharpening algorithms during the last decades [5]–[11]. The most widely used approaches are so-called component substitution (CS) methods, popularized because of their easy implementation and low computation cost in practical applications [11]–[13]. The basic assumption of CS methods is that the geometric detail information of an MS image lies in its structural component that can be obtained by transforming it into a new space. Then the structural component is substituted or partially substituted by a histogram matched version of PAN to inject the spatial information. Finally, pan-sharpening is achieved after an inverse transformation. The PCA based [14], [15], the IHS based [6], [12] and the Gram-Schmidt (GS) transform [16] based methods are those of the most widely known CS methods.

Another popular family is multi-resolution analysis (MRA) based methods. It has a well-known French name *amélioration de la résolution spatiale par injection de structures* (AR-SIS) [17], which means enhancement of the spatial resolution by structure injections. The MRA-based methods assume that the missing spatial information in MS can be inferred from the high frequency of the corresponding PAN image. To pan-sharpen an MS image, multi-resolution analysis algorithms, such as discrete wavelet transform (DWT) [18], à trous wavelet transform [19] or curvelet transform [20] are applied on a PAN image to extract high-frequency information and then inject it into the corresponding MS image.

In addition, pan-sharpening can be formulated as an inverse problem, in which PAN and MS images are considered as degraded versions of an HR MS image and it can be restored by resorting to some optimization procedures [21]–[23]. This is an ill-posed problem because much information has been lost during the degrading process. To obtain the optimal solution, regularizer [21] or prior knowledge [22] are added into formulations. Or, pan-sharpening can be addressed from the perspective of machine learning. For instance, Li et al. [24] and Zhu et al. [25], [26] modeled pan-sharpening from compressed sensing theory. Liu et al. [27] addressed pan-sharpening from a manifold learning framework.

Recently, deep learning techniques have achieved great success in diverse computer vision tasks [28]–[31], inspiring us to design deep learning models for the pan-sharpening problem. Observing that pan-sharpening and single image super-resolution share a similar spirit, and motivated by [28], Masi et al. [9] proposed a three-layered convolutional neural network (CNN) based pan-sharpening method and obtained improved results than traditional algorithms such as BSD3 [32] and

Qingjie Liu and Yunhong Wang are with the State Key Laboratory of Virtual Reality Technology and Systems, Beihang University and Hangzhou Innovation Institute, Beihang University. Email: {qingjie.liu, yhwang}@buaa.edu.cn. Yunhong Wang is the corresponding author of this paper.

Huanyu Zhou and Xiangyu Liu are with the School of the Computer Science and Engineering, Beihang University, Beijing, China. Email: xyliu@buaa.edu.cn

Qizhi Xu is with College of Information Science & Technology, Beijing University of Chemical Technology, Beijing, China. Email: qizhi@buct.edu.cn

Manuscript received April 19, 2020; revised August 26, 2020.

<sup>1</sup>Code and experimental results are available at this url:

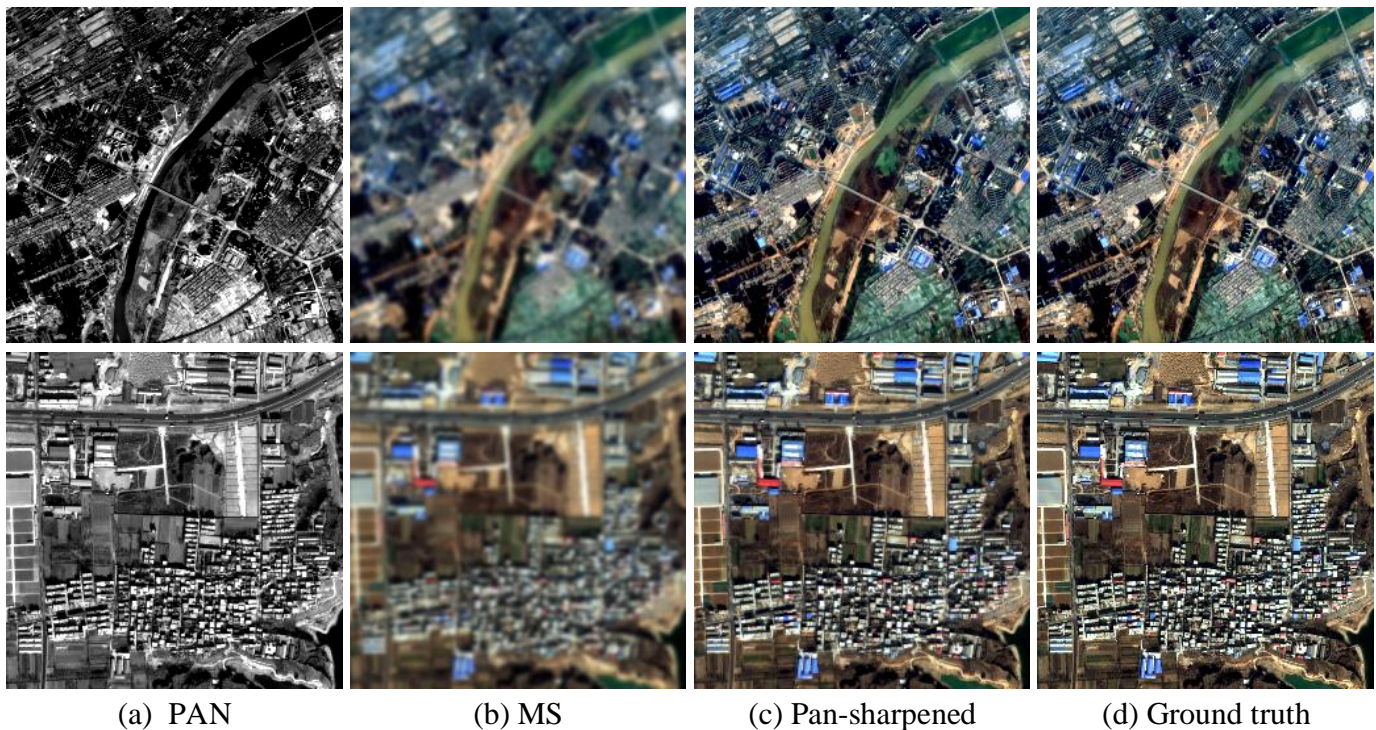


Fig. 1. Example results of the proposed method. (c) are high resolution MS images generated from (a) PAN and (b) MS. (d) are ground truth HR MS images.

AWLP [33]. Following this work, increasing attention has been paid to deep learning based pan-sharpening. For instance, Zhong et al. [34] presented a CNN based hybrid pan-sharpening method. Different from [9] that generate the pan-sharpened MS images directly, Zhong et al.'s work first enhances the spatial resolution of an input MS with the SRCNN method [28] and then applies GS transform on the enhanced MS and the PAN to accomplish the pan-sharpening. Rao et al. [35] proposed CNN based pan-sharpening model built on top of SRCNN, in which SRCNN was employed to learn the difference between up-sampled MS image and ground truth. The final results were obtained by adding the predicted difference image to the up-sampled MS. Similarly, Wei et al. [36] proposed a much deeper network (11 layers) to learn the residual images.

Recent studies [37], [38] have suggested that deeper networks will achieve better performance on vision tasks. However, training becomes very difficult with depth increasing. Residual learning [39] ease this problem by introducing shortcut connections between different layers of a network, allowing training networks much deeper than previous ones. Pan-sharpening could also be improved by residual learning. Although, Rao et al. [35] and Wei et al. [36] used the concept 'residual network', the networks employed in their methods are built with plain units. The depth of their networks is still shallow. The first attempt at applying the residual network is PanNet [40]. They adopt a similar idea to [35] and [36] but employ ResNet [39] to predict details of the image. In this way, both spatial and spectral information could be preserved well.

Although great advances have been made in this field, there

is still a great gap between the synthetic HR MS and the real one. It is still a challenging problem for researchers in the remote sensing community to obtain high spectral and spatial fidelity pan-sharpened images. To further boost the performance of pan-sharpening networks and obtain high-quality pan-sharpened images, in this paper we reformulate pan-sharpening as an image generation problem and explore the utilization of generative adversarial network (GAN) [41] to solve it. The GAN framework is a powerful generative model and was first introduced by Goodfellow et al. [41]. In contrast to previous networks that have a unified architecture, GANs have two individual components: one generator that is trained to generate images indistinguishable from real ones, and one discriminator that tries to distinguish whether the generated images are real or fake. With this perspective, this paper proposes PSGAN, a generative adversarial network that could produce high quality pan-sharpened images conditioned on the input of PAN and LR MS images.

This is an extension of our previous work [42], which is the first work that addresses the pan-sharpening problem from the perspective of generative adversarial learning. Compared with [42], background knowledge about GAN is presented. And we give more details about the architecture of the proposed PSGAN and evaluate several possible architecture configurations of the PSGAN. We enlarge the dataset and conduct extensive experiments to demonstrate the effectiveness and superiority of it. The main contributions of this paper are as follows:

- To the best of our knowledge, this is the first attempt at solving the pan-sharpening problem through generative adversarial learning.
- To accomplish pan-sharpening with the GAN framework,

we design a basic two-stream CNN architecture as the generator to produce high-quality pan-sharpened images and employ a fully convolutional discriminator to learn adaptive loss function for improving the quality of the pan-sharpened images.

- We evaluate various configurations of the proposed PSGAN and distill important factors that affect the performance of the pan-sharpening task.
- We demonstrate that the proposed PSGAN can produce astounding results on pan-sharpening problem. Fig. 1 shows one example result produced by our method.

The remainder of this paper is organized as follows: backgrounds and the theory of generative adversarial networks are briefly introduced in Section II. Section III formulates pan-sharpening from the perspective of generative adversarial learning and gives details of proposed PSGAN architecture. Experiments are conducted in Section IV. And finally this paper is concluded in Section V.

## II. GENERATIVE ADVERSARIAL NETWORKS

Given a set of unlabeled data, generative models aim at estimating their underlying distributions. This is a highly challenging task and inference on such distributions could be computationally expensive or even intractable. Recently proposed generative adversarial networks (GANs) [41] provide an efficient framework to learn generative models from unlabeled data.

GANs learn generative models by setting up an adversarial game between a generator neural network  $G$  and a discriminator neural network  $D$ . For any given data set  $\{\mathbf{x}\}$ , the generator  $G$  learns the distribution of the data by mapping a random sample  $\mathbf{z}$  from any distributions (e.g. Gaussian distribution or uniform distribution) to a sample  $\mathbf{x}$  from the data space. The  $G$  is trained to produce samples that can not be distinguished from the real samples. The discriminator  $D$  output a scalar indicating the probability that the samples are produced by  $G$  or it is from the real distribution. This process can be formulated as a two-player min-max game and written as follows:

$$\min_G \max_D V(D, G) = \mathbb{E}_{\mathbf{x} \sim p_{\text{data}}(\mathbf{x})} [\log D(\mathbf{x})] + \mathbb{E}_{\mathbf{z} \sim p_z(\mathbf{z})} [\log(1 - D(G(\mathbf{z})))] \quad (1)$$

where  $p_{\text{data}}(\mathbf{x})$  is the distribution of the real data,  $\mathbf{x}$  is a sample from  $p_{\text{data}}(\mathbf{x})$ . Correspondingly,  $p_z(\mathbf{z})$  is an arbitrary random distribution, and  $\mathbf{z}$  is a sample drawn from it. The first term of Eq. 1 indicates the probability of the discriminator determines a sample is a ‘real’ data, while the second term indicates the probability of the discriminator identify a samples is ‘fake’.  $D$  tries to assign correct labels to both real and generated data by maximizing the first term to 1 and the second term to 0. In contrast,  $G$  takes a random noise  $\mathbf{z}$  as input and tries to generate a sample that as indistinguishable from real one as possible by minimizing  $\log(1 - D(G(\mathbf{z})))$ . An illustration of this procedure is given in Fig. 2.

Eq. 1 can be optimized in an iterative way by fixing one parameter and optimizing another one. When  $G$  fixed, the

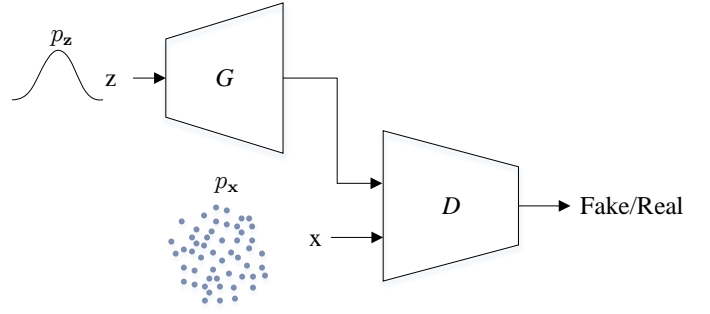


Fig. 2. An illustration of the generative adversarial framework.  $G$  is a generator accepting a random signal  $\mathbf{z}$  and trained to generate output that cannot be distinguished from a real data  $\mathbf{x}$  by a discriminator  $D$ .

optimization of  $D$  can be considered as maximizing the log-likelihood of the conditional probability  $p(Y = y|\mathbf{x})$ , where  $Y$  is the probability of sample  $\mathbf{x}$  comes from the real data ( $y = 1$ ) or the fake data ( $y = 0$ ). When  $D$  fixed, the objective of  $G$  is minimizing the Jensen-Shannon divergence between the real data distribution  $p_{\text{data}}$  and the fake data distribution  $p_G$  (here  $p_G$  denotes distribution learned by the generator  $G$ ). It can be proved that  $G$  has an optimal solution  $p_G = p_{\text{data}}$  [41]. And given enough capacity and training time, the generative neural network and the discriminator network will converge and achieve a point where the generator produce samples so real that the discriminator cannot distinguish them from the real data.

## III. PSGAN

### A. Formulation

Pan-sharpening aims to estimate a pan-sharpened HR MS image  $\hat{\mathbf{P}}$  from a LR MS image  $\mathbf{X}$  and a HR PAN image  $\mathbf{Y}$ . The output images should be as close as possible to the ideal HR MS images  $\mathbf{P}$ . We describe  $\mathbf{X}$  by a real-valued tensor of size  $w \times h \times b$ ,  $\mathbf{Y}$  by  $rw \times rh \times 1$ , and  $\hat{\mathbf{P}}$  and  $\mathbf{P}$  by  $rw \times rh \times b$  respectively, where  $r$  is the spatial resolution ratio between LR MS  $\mathbf{X}$  and HR PAN  $\mathbf{Y}$  (in this paper  $r = 4$ ) and  $b$  is the number of bands. The ultimate goal of pan-sharpening takes a general form as follows:

$$\hat{\mathbf{P}} = f(\mathbf{X}, \mathbf{Y}; \Theta) \quad (2)$$

where  $f(\cdot)$  is a pan-sharpening model which takes  $\mathbf{X}$  and  $\mathbf{Y}$  as input and produces desired HR MS  $\hat{\mathbf{P}}$ , and  $\Theta$  is collection of parameters for this model. Eq. (2) can be solved by minimizing the following loss function:

$$\hat{\Theta}_f = \arg \min \sum_{n=1}^N \ell [f_{\Theta}(\mathbf{X}_n, \mathbf{Y}_n), \mathbf{P}_n] \quad (3)$$

where  $N$  is the number of training samples. As an example, Eq. (2) can be realized from the perspective of compressed sensing, and Eq. (3) can be solved using dictionary learning algorithms [43].

From Eq. (4) we can see that  $f(\cdot)$  can be considered as a mapping function from  $(\mathbf{X}, \mathbf{Y})$  to  $\mathbf{P}$ . Thus, we can reformulate pan-sharpening as a conditional image generation problem that can be solved using conditional GAN [44]. Following [41] and [44], we define a generative network  $G$  that maps the

joint distribution  $p_{data}(\mathbf{X}, \mathbf{Y})$  to the target distribution  $p_r(\mathbf{P})$ . The generator  $G$  tries to produce pan-sharpened image  $\hat{\mathbf{P}}$  that cannot be distinguished from the reference image  $\mathbf{P}$  by an adversarial trained discriminative network  $D$ . This can be expressed as a mini-max game problem:

$$\min_{\Theta_G} \max_{\Theta_D} \mathbb{E}_{\mathbf{X} \sim p_{data}(\mathbf{X}), \mathbf{P} \sim p_r(\mathbf{P})} [\log D_{\Theta_D}(\mathbf{X}, \mathbf{P})] + \mathbb{E}_{(\mathbf{X}, \mathbf{Y}) \sim p_{data}(\mathbf{X}, \mathbf{Y})} [\log(1 - D_{\Theta_D}(\mathbf{X}, G_{\Theta_G}(\mathbf{X}, \mathbf{Y})))] \quad (4)$$

111111.....

### B. Architectures of the generator

The ultimate goal of a generator is producing a pan-sharpened MS image that cannot be distinguished from a real MS image. Since the inputs for a generator  $G$  are a HR PAN image and a LR MS image, there are multiple ways to design the  $G$ . One possible way is using the network architecture similar to PNN [9] which stacks the PAN and the upsampled MS to form a five-band input<sup>2</sup>. Another way is directly taking a two-stream design as in [45]. In this work, we devise and evaluate several generator architectures.

1) *Two-stream generator*: In contrast to other image generation tasks, e.g. single image super-resolution [46], image dehazing [47], or face aging [48], that learn one-to-one mappings, pan-sharpening accepts two images acquired by different sensors with distinct characteristics over the same scene. The two modalities, i.e., the PAN image and the MS image contain different information. PAN image is carrier of geometric detail (spatial) information, while MS image preserves spectral information. To make the best use of spatial and spectral information, we utilize two subnetworks to extract the hierarchical features of the input PAN and MS to capture complementary information of them. After that, the subsequent network proceeds as an auto-encoder: the encoder fuses information extracted from PAN and MS images, and the decoder reconstructs the HR MS images from the fused features in the final part.

Considering that the spatial resolution of MS images is only 1/4 of the desired pan-sharpened MS images, the pan-sharpening can be viewed as a special case of image super-resolution aided by PAN image. To enhance the spatial resolution of MS images using neural networks, there are usually two solutions. The *first* one is upscaling MS images to the desired size using some interpolation methods such as bicubic, and then applying neural networks to learn nonlinear mapping. The *second* one is applying the model directly without any preprocessing and performing up-scaling using networks. This will lead to deeper network structure and potentially better performance, however, with lower computational cost than previous one [49]. In this paper, we take consideration both of the two solutions.

**PSGAN** In our previous work [42], we employ the first solution to build the PSGAN, that is up-sampling the MS image firstly, and then feeding it and the corresponding PAN into two subnetworks for feature extraction. The architecture of the generator is shown in Fig. 3. The two subnetworks

have a similar structure but different weights. Each of them consists of two successive convolutional layers followed by a leaky rectified linear unit (LeakyReLU) [50] and a down-sampling layer. The convolutional layer with a stride of 2 instead of simple pooling strategy e.g. max pooling is used to down-sample the feature maps. After passing through the two subnetworks, the feature maps are first concatenated and then fused by subsequent convolutional layers. Finally, a decoder-like network architecture comprised of 2 transposed convolutional and 3 flat convolutional layers is applied to reconstruct the desired HR MS images. Inspired by the U-Net [51], we adapt the PSGAN network by adding skip connections. The skip connection will not only compensate details to higher layers but also ease the training. In the last layer, ReLU is used to guarantee the output is not negative.

**FU-PSGAN** We take PSGAN as base network and build variations on top of it. To differentiate different versions of PSGAN, we name the PSGAN with the second solution FU-PSGAN because the generator of it uses the **F**eature **U**p-scaling strategy. The generator of FU-PSGAN has almost identical architecture to PSGAN except that the MS subnetwork takes the original-sized MS as input and has one up convolution following the first convolution layer instead of a normal convolution layer, as shown in Fig. 4(a).

2) *PAN & MS Stacked generator*: Another possible way of designing generators is viewing the PAN and MS as a whole, i.e. stacking the two images along the channel dimension together to form a new image. To do this, the MS image should be up-sampled to match the size of the PAN image and then concatenated with the PAN to obtain an inflated image. One appealing advantage of this strategy is we can easily inherit some well-developed models from related research fields, such as single image super-resolution. For example, the pioneering PNN [9] borrows main structure of the network from SRCNN [28].

**ST-PSGAN** Following PNN [9], we design a deeper residual network to accomplish pan-sharpening. We call it ST-PSGAN since it has a **S**Tacked generator. The generator of ST-PSGAN is show in Fig. 4(b). It has almost the same structure to the generator of PSGAN in Fig. 3 except for one major difference that one stream, along with the skip connection binded on it, is removed to be consistent with the stacked PAN and MS. Another imperceptible change is that the first convolution layer should adapt to the channel dimension of the new input. For fair comparison, all the three PSGANs share the same discriminator which will be described below.

### C. Fully convolutional discriminator

In addition to a generator, a conditional discriminator network is trained simultaneously to discriminate the reference MS images from the generated pan-sharpened images. Similar to [44], we use a fully convolutional discriminator, which consists of five layers with kernels of  $3 \times 3$ . The stride of the first three layers are set to 2, and the last two is 1. Except for the last layer, all the convolution layers are activated through LeakyReLU. Sigmoid is used to predict the probability of being *real* HR MS or *pan-sharpened* MS for each input. The architecture of the discriminator is shown in Fig. 3.

<sup>2</sup>In this paper, we only consider 4-band MS images.

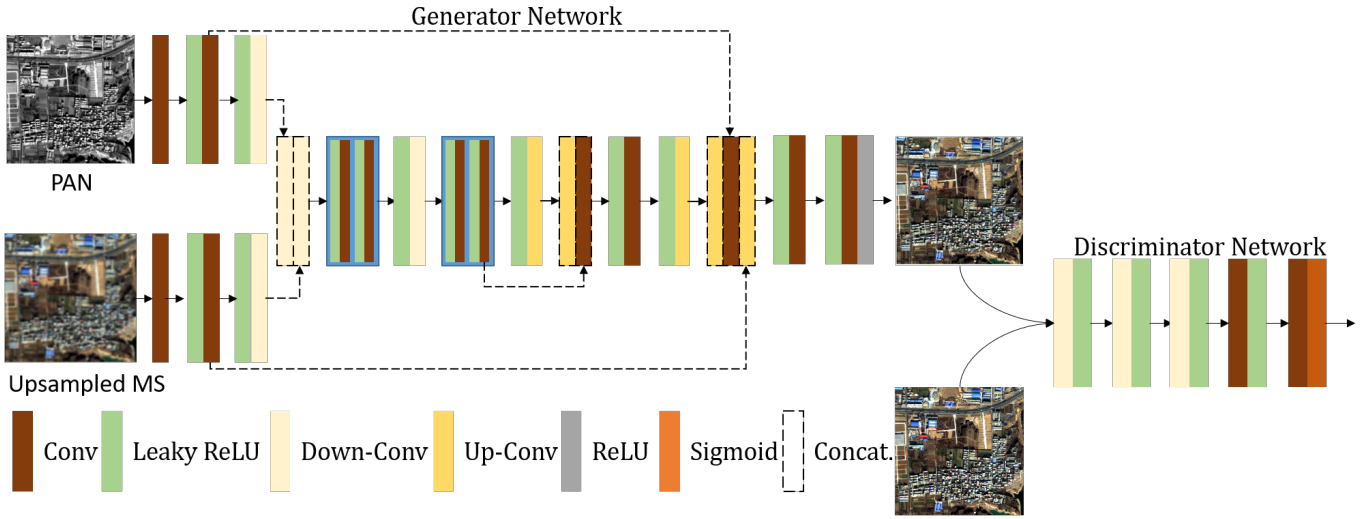


Fig. 3. Detailed architectures of the Generator network  $G$  and the Discriminator network  $D$ .

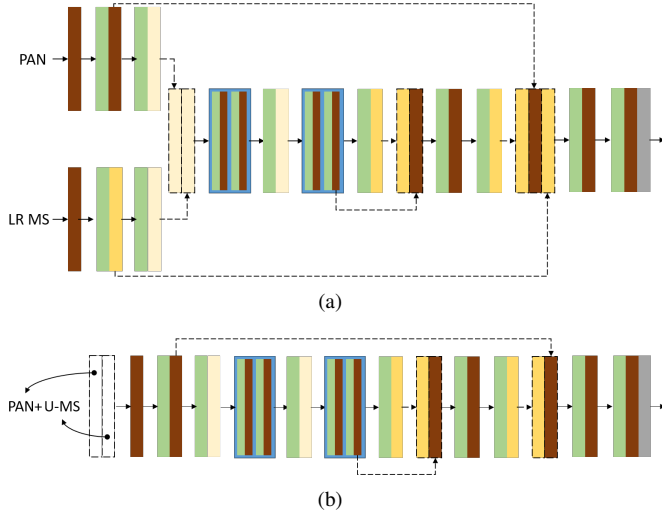


Fig. 4. Two variant generators for PSGANs. (a) is the generator performing up-scaling using networks; and (b) is the stacked generator that accepts one concatenated PAN and Upsampled MS (U-MS) image as input. The shape components here have the same means to Fig. 3.

#### D. Loss function

We train the three models using the same loss function. In this subsection, we will take PSGAN as an example to describe the loss function. The generative network  $G$  and the discriminator network  $D$  are trained alternately. To optimize  $G$  we adopt the pixel-wise loss and adversarial loss similar to some other state of the art GAN networks [44]. One common choice to In contrast to many previous works [9], [10] employing  $\ell_2$  loss that calculates mean squared errors between the ground truth and the reconstructed images, in this work, we adopt  $\ell_1$  loss that calculate the absolute difference between the pan-sharpened image and the ground truth.

To train the generative network  $G$ , many existing works employ  $\ell_2$  as loss function, which will result in blurring

effects. In this paper we adopt  $\ell_1$  to train  $G$ :

$$\mathcal{L}(G) = \sum_{n=1}^N [-\alpha \log D_{\Theta_D}(\mathbf{X}, G_{\Theta_G}(\mathbf{X}, \mathbf{Y})) + \beta \|\mathbf{P} - G_{\Theta_G}(\mathbf{X}, \mathbf{Y})\|_1] \quad (5)$$

Finally, the loss function for  $D$  takes the form:

$$\mathcal{L}(D) = \sum_{n=1}^N [1 - \log D_{\Theta_D}(\mathbf{X}, G_{\Theta_G}(\mathbf{X}, \mathbf{Y})) + \log D_{\Theta_D}(\mathbf{X}, \mathbf{P})] \quad (6)$$

where  $N$  is the number of training samples in a mini batch,  $\alpha$ ,  $\beta$  are hyper-parameters and are set to 1 and 100 in the experiments, respectively.

## IV. EXPERIMENTS

In this section, we conduct extensive experiments to evaluate the effectiveness and superiority of the proposed PSGANs.

### A. Dataset and implementation details

We train and test our networks on four datasets comprised of images acquired by QuickBird (QB) and GaoFen-1 (GF-1), GaoFen-2 (GF-2), and WorldView-2 (WV-2) satellites. Since the desired HR MS images are not available, we follow Wald's protocol [52] to down-sample both the MS and PAN images with a factor of  $r$  ( $r = 4$  in this paper). Then the original MS images are used as reference images to be compared with. We randomly crop patch pairs from the down-sampled MS and PAN to form training samples. It should be noted that we use larger patch size,  $64 \times 64 \times 4$  for MS patches and  $256 \times 256 \times 1$  for PAN patches, than our previous work [42], in which the sizes for MS and PAN patches are  $32 \times 32 \times 4$  and  $128 \times 128 \times 1$ , respectively. This will lead to smaller batch size during training, however, our experiments, which will be given in the next subsection, demonstrate that larger patch size produces better image quality. Brief information about the four datasets is illustrated in Table I. All the results reported in the following subsections are based on the test sets which are independent of the training images.

TABLE I  
BRIEF INFORMATION ABOUT THE FOUR DATASETS USED IN EXPERIMENTS.

Dataset	Images (Train/Test)	Training Samples	Spa. Res. (PAN/MS)
QB	9 (8/1)	25,038	0.6/2.4
GF-1	10 (9/1)	20,765	2.0/8.0
GF-2	9 (8/1)	13,460	0.8/3.2
WV-2	9 (8/1)	11,552	0.5/2.0

The PSGANs are implemented in PyTorch [53] and trained on a single NVIDIA Titan 1080Ti GPU. We use Adam optimizer [54] with an initial learning rate of 0.0002 and a momentum of 0.5 to minimize the loss function. The mini-batch size is set to 8. It takes about 10 hours to train one network.

### B. Evaluation indexes

We use five widely used metrics to evaluate the performance of the proposed and other methods on the four datasets, including SAM [57], CC, sCC [56], ERGAS [52], and Q<sub>4</sub> [55].

- **SAM** The *spectral angle mapper* (SAM) [57] measures spectral distortions of pan-sharpened images comparing with the reference images. It is defined as angles between the spectral vectors of pan-sharpened and reference images in the same pixel, which can be calculated as:

$$\text{SAM}(x_1, x_2) \triangleq \arccos \left( \frac{x_1 \cdot x_2}{\|x_1\| \cdot \|x_2\|} \right) \quad (7)$$

where  $x_1$  and  $x_2$  are two spectral vectors. SAM is averaged over all the images to generate a global measurement of spectral distortion. For the ideal pan-sharpened images, SAM should be 0.

- **CC** The *Correlation Coefficient* (CC) is another widely used indicator measuring the spectral quality of pan-sharpened images. It calculates the CC between a pan-sharpened image  $X$  and the corresponding reference image  $Y$  as

$$\text{CC} \triangleq \frac{\sum_{i=1}^w \sum_{j=1}^h (X_{i,j} - \mu_X)(Y_{i,j} - \mu_Y)}{\sqrt{\sum_{i=1}^w \sum_{j=1}^h (X_{i,j} - \mu_X)^2 \sum_{i=1}^w \sum_{j=1}^h (Y_{i,j} - \mu_Y)^2}} \quad (8)$$

where  $w$  and  $h$  are the width and height of the images,  $\mu_*$  indicates mean value of an image. CC ranges from -1 to +1, and the ideal value is +1.

- **sCC** To evaluate the similarity between the spatial details of pan-sharpened images and reference images, a high-pass filter is applied to obtain the high frequencies of them, then the correlation coefficient (CC) between the high frequencies is calculated. This quantity index is called *spatial CC* (sCC) [56]. We use the high Laplacian pass filter given by,

$$F = \begin{bmatrix} -1 & -1 & -1 \\ -1 & 8 & -1 \\ -1 & -1 & -1 \end{bmatrix} \quad (9)$$

to get the high frequency. A higher sCC indicates that most of the spatial information of the PAN image is injected during the fusion process. sCC is computed between each band of the pan-sharpened and reference image. The final sCC is averaged over all the bands of the MS images.

- **ERGAS** The *erreur relative globale adimensionnelle de synthèse* (ERGAS), also known as the relative global dimensional synthesis error is a commonly used global quality index [52]. It is given by,

$$\text{ERGAS} \triangleq 100 \frac{h}{l} \sqrt{\frac{1}{N} \sum_{i=1}^N \left( \frac{\text{RMSE}(B_i)}{M(B_i)} \right)^2} \quad (10)$$

where  $h$  and  $l$  are the spatial resolution of PAN and MS images;  $\text{RMSE}(B_i)$  is the root mean square error between the  $i$ th band of the fused and reference image;  $M(B_i)$  is the mean value of the original MS band  $B_i$ .

- **Q<sub>4</sub>** The *Quality-index* Q<sub>4</sub> [55] is the 4-band extension of Q index [58]. Q<sub>4</sub> is defined as:

$$Q_4 \triangleq \frac{4|\sigma_{z_1 z_2}| \cdot |\mu_{z_1}| \cdot |\mu_{z_2}|}{(\sigma_{z_1}^2 + \sigma_{z_2}^2)(\mu_{z_1}^2 + \mu_{z_2}^2)} \quad (11)$$

where  $z_1$  and  $z_2$  are two quaternions, formed with spectral vectors of MS images, i.e.  $z = a+ib+jc+kd$ ,  $\mu_{z_1}$  and  $\mu_{z_2}$  are the means of  $z_1$  and  $z_2$ ,  $\sigma_{z_1 z_2}$  denotes the covariance between  $z_1$  and  $z_2$ , and  $\sigma_{z_1}^2$  and  $\sigma_{z_2}^2$  are the variances of  $z_1$  and  $z_2$ .

Three non-reference metrics  $D_\lambda$ ,  $D_S$ , and QNR are employed for full resolution assessment.

- $D_\lambda$  [59] is a spectral quality indicator derived from the difference of inter-band  $Q$  values calculated from the pan-sharpened MS bands and the low-resolution MS bands. It is defined as:

$$D_\lambda \triangleq \sqrt{\frac{2}{K(K-1)} \sum_{i=1}^K \sum_{j=i}^K |Q(P_i, P_j) - Q(X_i, X_j)|} \quad (12)$$

where  $K$  is the number of bands for a MS image,  $P_i$  and  $X_i$  represent the  $i$ th band of the pan-sharpened and the LR MS images, respectively.

- $D_S$  [59] is a spatial quality metric complementary to  $D_\lambda$ . It is calculated as:

$$D_S \triangleq \sqrt{\frac{1}{K} \sum_{i=1}^K |Q(P_i, Y) - Q(X_i, \tilde{Y})|} \quad (13)$$

where  $Y$  is a PAN image and  $\tilde{Y}$  is its degraded low-resolution version. Both  $D_\lambda$  and  $D_S$  take values in [0,1], and the lower the better.

- **QNR** [59] is the abbreviation of *Quality with No Reference*. It is a combination of  $D_\lambda$  and  $D_S$  and measures global quality of fused images without any reference image. It is given by:

$$\text{QNR} \triangleq (1 - D_\lambda)(1 - D_S) \quad (14)$$

The ideal value of QNR is 1.

TABLE II

PERFORMANCE VARIATIONS WITH RESPECT TO PATCH SIZES. THE BATCH SIZE DECREASES FROM 32 TO 8 WITH PATCH SIZE INCREASES FROM 32 TO 64.

		Patch Size	SAM ↓	CC ↑	sCC ↑	ERGAS ↓	Q4 ↑
QB	PSGAN	32	1.2270	0.9867	0.9869	1.3594	0.9852
		64	1.1740	0.9877	0.9880	1.2602	0.9869
	FU-PSGAN	32	1.2883	0.9857	0.9861	1.3943	0.9845
		64	1.2411	0.9869	0.9865	1.2907	0.9864
	ST-PSGAN	32	1.3125	0.9867	0.9869	1.3662	0.9854
		64	1.2889	0.9869	0.9868	1.3267	0.9857
GF-2	PSGAN	32	0.7484	0.9908	0.9929	0.7303	0.9981
		64	0.7575	0.9909	0.9929	0.7233	0.9980
	FU-PSGAN	32	0.7456	0.9909	0.9931	0.7214	0.9982
		64	0.7181	0.9915	0.9935	0.7013	0.9982
	ST-PSGAN	32	0.7856	0.9903	0.9924	0.7477	0.9980
		64	0.7300	0.9913	0.9933	0.7084	0.9981

TABLE III

IMPACTS OF BATCH NORMALIZATION AND SELF-ATTENTION ON THE FOUR DATASETS. '+BN' MEANS PSGAN IS MODIFIED BY ADDING BATCH NORMALIZATION AFTER EACH CONVOLUTION BLOCK. '+SA' MEANS PSGAN IS EQUIPPED WITH SELF-ATTENTION.

		SAM ↓	CC ↑	sCC ↑	ERGAS ↓	Q4 ↑
QB	PSGAN	1.1740	0.9877	0.9880	1.2602	0.9869
	PSGAN+BN	9.2521	0.9274	0.9075	14.029	0.8167
	PSGAN+SA	2.1396	0.9696	0.9738	2.3140	0.9629
GF-1	PSGAN	0.6086	0.9898	0.9921	0.5423	0.9924
	PSGAN+BN	2.5698	0.9537	0.9593	15.432	0.8110
	PSGAN+SA	3.8799	0.8655	0.8842	7.0921	0.4662
GF-2	PSGAN	0.7575	0.9909	0.9929	0.7233	0.9980
	PSGAN+BN	1.5903	0.9669	0.9698	7.6059	0.9260
	PSGAN+SA	1.2182	0.9739	0.9793	1.2422	0.9944
WV-2	PSGAN	0.9127	0.9973	0.9975	1.6452	0.9971
	PSGAN+BN	8.1520	0.8697	0.8448	9.6634	0.8016
	PSGAN+SA	1.4185	0.9950	0.9943	2.2273	0.9944

### C. Impact of patch size

In our previous work [42], we use small patch size to generate training samples, which allows us to set a larger batch size and thus enables more stable training and faster convergence [60]. However, for image reconstruction tasks, larger patch size is beneficial for generating high-quality images. In this paper, we test a much larger patch size than [42]. Although the batch size will decrease accordingly, our experiments demonstrate that larger patches lead to higher image quality. We conduct experiments on the QB and GF-2 images to evaluate how much the impact will be by setting different patch sizes. The results are given in Table II, from which we can see patch size does have a positive impact on the image quality. For all three models, the image quality has a significant improvement when using the 64 patch size, even though the batch is decreased from 32 to 8.

### D. Batch normalization is harmful

Batch normalization (BN) [61] has been widely used in neural networks to stabilize and accelerate trainings. It also has been applied to the pan-sharpening task for improving performance [62], [63]. However, recent studies have suggested that batch normalization may be unnecessary in low level visions [64]. It brings two burdens: firstly, BN operation

requires amount of storage and computational resources, which could be used to add more convolutional layers. Secondly, BN layers get rid of scale information, which is helpful for recognition tasks, however, is harmful for scale-sensitive tasks, such as image super-resolution and pan-sharpening. We add a BN layer after each convolution layer for comparison. The results are given in Table III. We can observe that adding BN layers severely decrease the performance, especially on the QB and WV-2 images. Thus, in this work we remove all the BN layers from our models.

### E. Self-attention is not useful

Attention plays an important role in human perception. It allows human brain to selectively concentrate on information meaningful to perceive tasks, while ignoring other irrelative information. Since it was introduced to the deep learning [73], the attention mechanism has become one of the most valuable breakthroughs in the community and significantly boosts a variety of AI tasks ranging from NLP [74] to CV [75] domains.

Self-attention (SA) has been reported to be able to generate high-quality images when incorporating with GANs [75]. Thus, in this paper, we explore to leverage the SA module to improve PSGAN. The experimental results are illustrated in Table III, from which we can see that on the QB and WV-2 images, the PSGAN+SA obtains satisfactory performance. It has a comparable spatial quality to the original PSGAN. The GF-1 and GF-2 images are challenges to the self-attention. All metrics are much poor than the PSGAN except for the Q4 on the GF-2. PSGAN+SA works slightly worse.

### F. Two-stream is better than stacking

We present two variants of our PSGAN, i.e., FU-PSGAN and ST-PSGAN. PSGAN and FU-PSGAN share the similar structure that both have two-stream inputs as described in Section III-B1. ST-PSGAN has only one input branch that accept stacked PAN and up-sampled MS as input. Most previous works adopt a one branch design similar to ST-PSGAN, such as PNN [9] and PanNet [10]. Here, we test which one is a better solution. We test these three models on the four datasets, and report results on Tables IV to VI. As can be seen, although ST-PSGAN achieves the best results on

TABLE IV  
PERFORMANCE COMPARISONS ON THE TEST SET OF QB. THE TOP THREE PERFORMANCES ARE HIGHLIGHTED WITH RED, GREEN, AND BLUE

	SAM↓	CC↑	sCC↑	ERGAS↓	Q4↑	$D_\lambda$ ↓	$D_S$ ↓	QNR↑
SFIM [65]	1.3465	0.9620	0.9752	2.6051	0.9643	<b>0.0062</b>	0.0170	0.9769
LMVM [66]	1.7131	0.9694	0.9703	2.3509	0.9647	<b>0.0020</b>	0.0164	<b>0.9816</b>
LMM [66]	1.6845	0.9634	0.9695	2.4306	0.9640	0.0064	0.0173	0.9763
HPF [67]	1.3522	0.9699	0.9811	2.2534	0.9698	0.0069	0.0178	0.9755
HPFC [67]	1.6558	0.9609	0.9776	4.2814	0.9453	0.0461	0.0468	0.9093
Brovey [68]	1.4782	0.9729	0.9720	2.0542	0.9735	0.0281	0.0503	0.9231
HCS [69]	1.4782	0.9729	0.9685	2.5003	0.9632	0.0137	0.0285	0.9582
IHS [70]	1.6100	0.9683	0.9822	2.2611	0.9697	0.0078	0.0550	0.9376
GS [71]	1.3063	0.9726	0.9821	2.1309	0.9704	0.0232	0.0497	0.9283
BDSB [72]	1.4725	0.9725	0.9864	2.2722	0.9707	0.0147	0.0227	0.9629
PNN [9]	2.0777	0.9731	0.9718	1.8752	0.9723	0.0273	0.0278	0.9457
PanNet [10]	<b>1.1068</b>	0.9848	<b>0.9877</b>	1.3800	0.9834	<b>0.0019</b>	<b>0.0111</b>	<b>0.9871</b>
PSGAN	<b>1.1740</b>	<b>0.9877</b>	<b>0.9880</b>	<b>1.2602</b>	<b>0.9869</b>	0.0067	<b>0.0116</b>	<b>0.9818</b>
FU-PSGAN	<b>1.2411</b>	<b>0.9869</b>	0.9865	<b>1.2907</b>	<b>0.9864</b>	0.0104	<b>0.0149</b>	0.9749
ST-PSGAN	1.2889	<b>0.9869</b>	<b>0.9868</b>	<b>1.3267</b>	<b>0.9857</b>	0.0138	0.0162	0.9702

TABLE V  
PERFORMANCE COMPARISONS ON THE TEST SET OF GF-2. THE TOP THREE PERFORMANCES ARE HIGHLIGHTED WITH RED, GREEN, AND BLUE

	SAM↓	CC↑	sCC↑	ERGAS↓	Q4↑	$D_\lambda$ ↓	$D_S$ ↓	QNR↑
SFIM [65]	1.5584	0.8721	0.9512	2.8705	0.8786	0.0123	0.0446	0.9437
LMVM [66]	2.0111	0.9073	0.9365	2.3138	0.9037	0.0022	0.0304	0.9675
LMM [66]	1.5527	0.8406	0.9450	3.0812	0.8387	0.0151	0.0508	0.9349
HPF [67]	1.5642	0.8776	0.9645	2.7818	0.8779	0.0118	0.0425	0.9462
HPFC [67]	1.7647	0.8852	0.9600	3.9200	0.8764	0.0840	0.0899	0.8337
Brovey [68]	1.3407	0.7990	0.9049	3.2624	0.8056	0.0454	0.1693	0.7930
HCS [69]	1.3407	0.8376	0.9392	3.2678	0.8296	0.0200	0.0615	0.9197
IHS [70]	1.8277	0.8109	0.9236	3.3495	0.8168	0.0530	0.1617	0.7938
GS [71]	2.2288	0.7898	0.8947	3.4247	0.7861	0.0819	0.1736	0.7587
BDSB [72]	1.8392	0.8791	0.9512	2.8705	0.8786	0.0066	0.0523	0.9415
PNN [9]	1.1899	0.9749	0.9821	1.2172	0.9946	0.0111	0.0494	0.9400
PanNet [10]	0.9370	0.9864	0.9889	0.8902	0.9971	0.0051	0.0128	0.9822
PSGAN	<b>0.7575</b>	<b>0.9909</b>	<b>0.9929</b>	<b>0.7233</b>	<b>0.9980</b>	<b>0.0019</b>	<b>0.0060</b>	<b>0.9921</b>
FU-PSGAN	<b>0.7181</b>	<b>0.9915</b>	<b>0.9935</b>	<b>0.7013</b>	<b>0.9982</b>	<b>0.0020</b>	<b>0.0089</b>	<b>0.9892</b>
ST-PSGAN	<b>0.7300</b>	<b>0.9913</b>	<b>0.9933</b>	<b>0.7084</b>	<b>0.9981</b>	<b>0.0008</b>	<b>0.0070</b>	<b>0.9922</b>

TABLE VI  
PERFORMANCE COMPARISONS ON THE TEST SET OF GF-1 AND WV2.

	SAM↓	CC↑	sCC↑	ERGAS↓	Q4↑	$D_\lambda$ ↓	$D_S$ ↓	QNR↑	
GF-1	PNN [9]	2.1381	0.9659	0.9752	1.4434	0.9603	0.0435	<b>0.0155</b>	0.9416
	PanNet [10]	0.6616	0.9850	0.9882	0.6409	0.9888	0.0173	0.0267	0.9564
	PSGAN	<b>0.6086</b>	<b>0.9898</b>	<b>0.9921</b>	<b>0.5423</b>	<b>0.9924</b>	<b>0.0040</b>	<b>0.0172</b>	<b>0.9789</b>
	FU-PSGAN	<b>0.6229</b>	<b>0.9898</b>	<b>0.9923</b>	<b>0.5436</b>	<b>0.9925</b>	<b>0.0111</b>	0.0273	<b>0.9655</b>
	ST-PSGAN	0.8310	<b>0.9895</b>	0.9919	0.5831	0.9917	0.0153	0.0282	0.9570
WV-2	PNN [9]	1.4746	0.9955	0.9950	2.1630	0.9951	0.0086	0.0120	0.9795
	PanNet [10]	0.9810	0.9966	0.9966	1.8530	0.9964	0.0044	0.0103	0.9854
	PSGAN	<b>0.9127</b>	<b>0.9973</b>	<b>0.9975</b>	<b>1.6452</b>	<b>0.9971</b>	0.0021	<b>0.0045</b>	<b>0.9934</b>
	FU-PSGAN	<b>0.8855</b>	<b>0.9974</b>	<b>0.9974</b>	<b>1.6319</b>	<b>0.9971</b>	<b>0.0016</b>	<b>0.0038</b>	<b>0.9947</b>
	ST-PSGAN	0.9280	0.9972	0.9973	1.6872	<b>0.9970</b>	<b>0.0018</b>	0.0085	0.9897

GF-2 dataset w.r.t.  $D_\lambda$ , and QNR, it is inferior to two-stream models, which indicates two-stream architecture does perform better than stacking input.

### G. Comparison with other pan-sharpening methods

In this subsection, we compare the proposed PSGAN and two improved variations, i.e. FU-PSGAN and ST-PSGAN with twelve widely used pan-sharpening techniques, including ten traditional methods: SFIM [65], LMVM [66], LMM [66], HPF [67], HPFC [67], Brovey [68], HCS [69], IHS [11], GS [71], BDSB [72], and two deep learning based methods: PNN [9] and PanNet [10]. Tables IV to VI list the quantitative evaluations on the four datasets w.r.t. eight metrics. Tables IV and V report quality indexes of all comparison methods. It

can be seen deep models achieve very good performance and even are superior to traditional methods in most cases. PanNet [10] is a successful method with very promising results. It obtains the best SAM on QB images and generalizes well to full scale images, which is supported by its optimal no reference metrics. As a pioneering deep model, PNN [9] proves the effectiveness of applying deep neural networks to pan-sharpening tasks. Although PNN has the lowest spectral quality on QB dataset, it works well on GF-2 images with surprisingly good SAM surpassing all traditional methods. The proposed PSGAN obtains the best metrics on the QB images except for the SAM and three non-reference indicators. On GF-2 dataset, PSGAN and its variants shows superiority performance than all other methods. Especially, increasing the



spatial resolution of MS images using CNN networks, i.e., FU-PSGAN gains the best performance. Stacking the MS and PAN images together to perform pan-sharpening achieve the second best place on GF-2 dataset, however it fall behind other two PSGAN models. In summary, the two-stream strategy is better than the stacking one.

Table VI presents quantitative results on GF-1 and WV-2 images. On these two datasets, we only lists the results of the deep models. As can be observed, our models still perform better than the other two deep methods. And the FU-PSGAN achieves the best results on WV-2 images with the highest SAM, CC, ERGAS, and  $Q_4$ , and slightly worse sCC than PSGAN. Its results on GF-1 are also promising, with much comparable performance to PSGAN and much better performance than PNN, PanNet, and ST-PSGAN.

#### H. Visual comparisons

Figs. 5 and 6 and ??? shows sample results cropped from the test site of Quickbird, GF-2, WorldView-2, and GF-1, respectively. All images are displayed in true color (RGB). In Figs. 5 and 6, LMVM [66] and PNN [9] produce images with obvious blurring. Brovey [68], IHS [11], GS [71], and BDSF [72] returns results similar to the reference images with fine spatial details, but suffers from strong spectral distortions. The results of PCNN [9] are similar to ours, but some missing spatial details are noticeable. PSGAN produces the best results with less blurring and reduced spectral distortions.

#### I. Experiments on full resolution images

### V. CONCLUSION

In this paper, we have proposed PSGAN that consists of a two-stream fusion network as generator and a patch discriminator to solve the pan-sharpening problem. The experiments on different sensors demonstrate the effectiveness of the proposed method, and comparisons with other methods also shows great superiority of it. In the future, we would like to apply deeper network such as residual neural network to our approach. We will also explore the generalization of the model by testing it on the data from satellites which are never used to train.

### REFERENCES

- [1] David J Mulla, "Twenty five years of remote sensing in precision agriculture: Key advances and remaining knowledge gaps," *Biosystems engineering*, vol. 114, no. 4, pp. 358–371, 2013.
- [2] Adel Shalaby and Ryutaro Tateishi, "Remote sensing and gis for mapping and monitoring land cover and land-use changes in the northwestern coastal zone of egypt," *Appl. Geogr.*, vol. 27, no. 1, pp. 28–41, 2007.
- [3] Qihao Weng, "Thermal infrared remote sensing for urban climate and environmental studies: Methods, applications, and trends," *ISPRS J. Photogramm. Remote Sens.*, vol. 64, no. 4, pp. 335–344, 2009.
- [4] Yun Zhang, "Understanding image fusion," *PE&RS*, vol. 70, no. 6, pp. 657–661, 2004.
- [5] Claire Thomas, Thierry Ranchin, Lucien Wald, et al., "Synthesis of multispectral images to high spatial resolution: A critical review of fusion methods based on remote sensing physics," *IEEE Trans. Geosci. Remote Sens.*, vol. 46, no. 5, pp. 1301–1312, 2008.
- [6] Qizhi Xu, Bo Li, Yun Zhang, and Lin Ding, "High-fidelity component substitution pansharpening by the fitting of substitution data," *IEEE Trans. Geosci. Remote Sens.*, vol. 52, no. 11, pp. 7380–7392, 2014.
- [7] Gemine Vivone, Luciano Alparone, Jocelyn Chanussot, et al., "A critical comparison among pansharpening algorithms," *IEEE Trans. Geosci. Remote Sens.*, vol. 53, no. 5, pp. 2565–2586, 2015.
- [8] Hassan Ghassemian, "A review of remote sensing image fusion methods," *Inf. Fusion*, vol. 32, pp. 75–89, 2016.
- [9] Giuseppe Masi, Davide Cozzolino, Luisa Verdoliva, et al., "Pansharpening by convolutional neural networks," *Remote Sens.*, vol. 8, no. 7, pp. 594, 2016.
- [10] Junfeng Yang, Xueyang Fu, Yuwen Hu, Yue Huang, Xinghao Ding, and John Paisley, "Pannet: A deep network architecture for pan-sharpening," in *Pro. Int. Conf. Comput. Vis.* 2017, pp. 5449–5457, IEEE.
- [11] Sheida Rahmani, Melissa Strait, Daria Merkurjev, et al., "An adaptive ihs pan-sharpening method," *IEEE Geosci. Remote Sens. Lett.*, vol. 7, no. 4, pp. 746–750, 2010.
- [12] Te-Ming Tu, Shun-Chi Su, Hsuen-Chyun Shyu, and Ping S Huang, "A new look at ihs-like image fusion methods," *Inf. Fusion*, vol. 2, no. 3, pp. 177–186, 2001.
- [13] Te-Ming Tu, Ping Sheng Huang, Chung-Ling Hung, and Chien-Ping Chang, "A fast intensity-hue-saturation fusion technique with spectral adjustment for ikonos imagery," *IEEE Geosci. Remote Sens. Lett.*, vol. 1, no. 4, pp. 309–312, 2004.
- [14] Pats Chavez, Stuart C Sides, Jeffrey A Anderson, et al., "Comparison of three different methods to merge multiresolution and multispectral data-Landsat TM and SPOT panchromatic," *Photogramm. Eng. Remote Sens.*, vol. 57, no. 3, pp. 295–303, 1991.
- [15] Hamid Reza Shahdoosti and Hassan Ghassemian, "Combining the spectral pca and spatial pca fusion methods by an optimal filter," *Inf. Fusion*, vol. 27, pp. 150–160, 2016.
- [16] Craig A Laben and Bernard V Brower, "Process for enhancing the spatial resolution of multispectral imagery using pan-sharpening," Jan. 4 2000, US Patent 6,011,875.
- [17] Thierry Ranchin and Lucien Wald, "Fusion of high spatial and spectral resolution images: The ARSIS concept and its implementation," *Photogramm. Eng. Remote Sens.*, vol. 66, no. 1, pp. 49–61, 2000.
- [18] Pushkar S Pradhan, Roger L King, Nicolas H Younan, et al., "Estimation of the number of decomposition levels for a wavelet-based multiresolution multisensor image fusion," *IEEE Trans. Geosci. Remote Sens.*, vol. 44, no. 12, pp. 3674–3686, 2006.
- [19] Jorge Nunez, Xavier Otazu, Octavi Fors, et al., "Multiresolution-based image fusion with additive wavelet decomposition," *IEEE Trans. Geosci. Remote Sens.*, vol. 37, no. 3, pp. 1204–1211, 1999.
- [20] Filippo Nencini, Andrea Garzelli, Stefano Baronti, and Luciano Alparone, "Remote sensing image fusion using the curvelet transform," *Inf. Fusion*, vol. 8, no. 2, pp. 143–156, 2007.
- [21] Chen Chen, Yeqing Li, Wei Liu, and Junzhou Huang, "Image fusion with local spectral consistency and dynamic gradient sparsity," in *Proc. Comput. Vis. and Pattern Recog.* IEEE, 2014, pp. 2760–2765.
- [22] Xiyan He, Laurent Condat, José M Bioucas-Dias, et al., "A new pansharpening method based on spatial and spectral sparsity priors," *IEEE Trans. Image Process.*, vol. 23, no. 9, pp. 4160–4174, 2014.
- [23] Gemine Vivone, Miguel Simões, Mauro Dalla Mura, Rocco Restaino, José M Bioucas-Dias, Giorgio A Licciardi, and Jocelyn Chanussot, "Pansharpening based on semiblind deconvolution," *IEEE Trans. Geosci. Remote Sens.*, vol. 53, no. 4, pp. 1997–2010, 2015.
- [24] Shutao Li and Bin Yang, "A new pan-sharpening method using a compressed sensing technique," *IEEE Trans. Geosci. Remote Sens.*, vol. 49, no. 2, pp. 738–746, 2011.
- [25] Xiao Xiang Zhu and Richard Bamler, "A sparse image fusion algorithm with application to pan-sharpening," *IEEE Trans. Geosci. Remote Sens.*, vol. 51, no. 5, pp. 2827–2836, 2013.
- [26] Xiao Xiang Zhu, Claas Grohnfeldt, and Richard Bamler, "Exploiting joint sparsity for pansharpening: the J-SparseFI algorithm," *IEEE Trans. Geosci. Remote Sens.*, vol. 54, no. 5, pp. 2664–2681, 2016.
- [27] Qingjie Liu, Yunhong Wang, and Zhaoxiang Zhang, "Pan-sharpening based on geometric clustered neighbor embedding," *Opt. Eng.*, vol. 53, no. 9, pp. 093109–093109, 2014.
- [28] Chao Dong, Chen Change Loy, Kaïming He, et al., "Image super-resolution using deep convolutional networks," *IEEE Trans. Pattern Anal. Mach. Intell.*, vol. 38, no. 2, pp. 295–307, 2016.
- [29] Qinchuan Zhang, Yunhong Wang, Qingjie Liu, et al., "CNN based suburban building detection using monocular high resolution google earth images," in *Proc. IGARSS*, 2016, pp. 661–664.
- [30] Suhas Sreehari, SV Venkatakrisnan, Katherine L Bouman, et al., "Multi-resolution data fusion for super-resolution electron microscopy," in *Proc. Comput. Vis. Pattern Recog. Workshop.* IEEE, 2017, pp. 1084–1092.
- [31] Christian Ledig, Lucas Theis, Ferenc Huszár, et al., "Photo-realistic single image super-resolution using a generative adversarial network," in *Proc. Comput. Vis. Pattern Recog.*, 2017, pp. 4681–4690.

- [32] Andrea Garzelli, Filippo Nencini, and Luca Capobianco, "Optimal mmse pan sharpening of very high resolution multispectral images," *IEEE Trans. Geosci. Remote Sens.*, vol. 46, no. 1, pp. 228–236, 2008.
- [33] Xavier Otazu, María González-Audícana, Octavi Fors, et al., "Introduction of sensor spectral response into image fusion methods. application to wavelet-based methods," *IEEE Trans. Geosci. Remote Sens.*, vol. 43, no. 10, pp. 2376–2385, 2005.
- [34] Jinying Zhong, Bin Yang, Guoyu Huang, et al., "Remote sensing image fusion with convolutional neural network," *Sensing and Imaging*, vol. 17, no. 1, pp. 10, 2016.
- [35] Yizhou Rao, Lin He, and Jiawei Zhu, "A residual convolutional neural network for pan-sharpening," in *International Workshop on Remote Sensing with Intelligent Processing (RSIP)*. IEEE, 2017, pp. 1–4.
- [36] Yancong Wei, Qiangqiang Yuan, Huanfeng Shen, and Liangpei Zhang, "Boosting the accuracy of multispectral image pansharpening by learning a deep residual network," *IEEE Geosci. Remote Sens. Lett.*, vol. 14, no. 10, pp. 1795–1799, 2017.
- [37] Christian Szegedy, Wei Liu, Yangqing Jia, Pierre Sermanet, Scott Reed, Dragomir Anguelov, Dumitru Erhan, Vincent Vanhoucke, and Andrew Rabinovich, "Going deeper with convolutions," in *Proc. Comput. Vis. Pattern Recog.* IEEE, 2015, pp. 1–9.
- [38] Karen Simonyan and Andrew Zisserman, "Very deep convolutional networks for large-scale image recognition," in *Proc. ICLR*, 2015.
- [39] Kaiming He, Xiangyu Zhang, Shaoqing Ren, et al., "Deep residual learning for image recognition," in *Proc. Comput. Vis. Pattern Recog.*, 2016, pp. 770–778.
- [40] Junfeng Yang, Xueyang Fu, Yuwen Hu, et al., "PanNet: A deep network architecture for pan-sharpening," in *Proc. Int. Conf. Comput. Vis.*, 2017, pp. 5449–5457.
- [41] Ian Goodfellow, Jean Pouget-Abadie, Mehdi Mirza, et al., "Generative adversarial nets," in *Proc. NIPS*, 2014, pp. 2672–2680.
- [42] Xiangyu Liu, Yunhong Wang, and Qingjie Liu, "PSGAN: A generative adversarial network for remote sensing image pan-sharpening," in *Proc. Int. Conf. Image Process.* IEEE, 2018, pp. 1–5.
- [43] Jin Xie, Yue Huang, John Paisley, et al., "Pan-sharpening based on nonparametric bayesian adaptive dictionary learning," in *Proc. ICIP*, 2013, pp. 2039–2042.
- [44] Phillip Isola, Jun-Yan Zhu, Tinghui Zhou, et al., "Image-to-image translation with conditional adversarial networks," in *Proc. Comput. Vis. Pattern Recog.*, 2017, pp. 1125–1134.
- [45] Xiangyu Liu, Qingjie Liu, and Yunhong Wang, "Remote sensing image fusion based on two-stream fusion network," *Inf. Fusion*, vol. 55, pp. 1–15, 2020.
- [46] Christian Ledig, Lucas Theis, Ferenc Huszar, Jose Caballero, Andrew Cunningham, Alejandro Acosta, Andrew Aitken, Alykhan Tejani, Johannes Totz, Zehan Wang, and Wenzhe Shi, "Photo-realistic single image super-resolution using a generative adversarial network," in *Proc. Comput. Vis. Pattern Recog.*, July 2017.
- [47] Yanyun Qu, Yizi Chen, Jingying Huang, and Yuan Xie, "Enhanced pix2pix dehazing network," in *Proc. Comput. Vis. Pattern Recog.*, June 2019.
- [48] Hongyu Yang, Di Huang, Yunhong Wang, and Anil K Jain, "Learning continuous face age progression: A pyramid of gans," *IEEE Trans. Pattern Anal. Mach. Intell.*, 2019.
- [49] Chao Dong, Chen Change Loy, and Xiaoou Tang, "Accelerating the super-resolution convolutional neural network," in *Proc. ECCV*. Springer, 2016, pp. 391–407.
- [50] Andrew L. Maas, Awni Y. Hannun, and Andrew Y. Ng, "Rectifier nonlinearities improve neural network acoustic models," in *Proc. ICML*, 2013, vol. 30, p. 3.
- [51] Olaf Ronneberger, Philipp Fischer, and Thomas Brox, "U-Net: Convolutional networks for biomedical image segmentation," in *Proc. MICCAI*, 2015, pp. 234–241.
- [52] Lucien Wald, "Quality of high resolution synthesised images: Is there a simple criterion?," in *Proceedings of the Fusion of Earth Data: Merging Point Measurements, Raster Maps, and Remotely Sensed image*, 2000, pp. 99–103.
- [53] Adam Paszke, Sam Gross, Francisco Massa, Adam Lerer, James Bradbury, Gregory Chanan, Trevor Killeen, Zeming Lin, Natalia Gimelshein, Luca Antiga, et al., "Pytorch: An imperative style, high-performance deep learning library," in *Advances in Neural Information Processing Systems*, 2019, pp. 8024–8035.
- [54] Diederik P Kingma and Jimmy Ba, "Adam: A method for stochastic optimization," in *Proc. ICLR*, 2015.
- [55] Zhou Wang, Bovik Alan, C. and Ligang Lu, "A universal image quality index," *Signal Process. Lett.*, vol. 9, no. 2, pp. 81–84, 2002.
- [56] J Zhou, DL Civco, and JA Silander, "A wavelet transform method to merge landsat tm and spot panchromatic data," *Int. J. Remote Sens.*, vol. 19, no. 4, pp. 743–757, 1998.
- [57] R. H. Yuhas, A. F. H. Goetz, and J.W. Boardman, "Discrimination among semi-arid landscape endmembers using the spectral angle mapper (SAM) algorithm," in *Proc. Summaries 3rd Annu. JPL Airborne Geosci. Workshop*, Jun. 1992, pp. 147 – 149.
- [58] Lucien Wald, Thierry Ranchin, and Marc Mangolini, "Fusion of satellite images of different spatial resolutions: Assessing the quality of resulting images," *Photogramm. Eng. Remote Sens.*, vol. 63, pp. 691–699, 1997.
- [59] Luciano Alparone, Bruno Aiazzi, Stefano Baronti, Andrea Garzelli, Filippo Nencini, and Massimo Selva, "Multispectral and panchromatic data fusion assessment without reference," *Photogramm. Eng. Remote Sens.*, vol. 74, no. 2, pp. 193–200, 2008.
- [60] Priya Goyal, Piotr Dollár, Ross Girshick, Pieter Noordhuis, Lukasz Wesolowski, Aapo Kyrola, Andrew Tulloch, Yangqing Jia, and Kaiming He, "Accurate, large minibatch sgd: Training imagenet in 1 hour," *arXiv preprint arXiv:1706.02677*, 2017.
- [61] Sergey Ioffe and Christian Szegedy, "Batch normalization: Accelerating deep network training by reducing internal covariate shift," *arXiv preprint arXiv:1502.03167*, 2015.
- [62] Giuseppe Scarpa, Sergio Vitale, and Davide Cozzolino, "Target-adaptive cnn-based pansharpening," *IEEE Trans. Geosci. Remote Sens.*, vol. 56, no. 9, pp. 5443–5457, 2018.
- [63] Renwei Dian, Shutao Li, Anjing Guo, and Leyuan Fang, "Deep hyperspectral image sharpening," *IEEE Trans. Neural Netw. Learn. Syst.*, no. 99, pp. 1–11, 2018.
- [64] Bee Lim, Sanghyun Son, Heewon Kim, Seungjun Nah, and Kyoung Mu Lee, "Enhanced deep residual networks for single image super-resolution," in *Proc. Comput. Vis. Pattern Recog. Workshops*, 2017, pp. 136–144.
- [65] JG Liu, "Smoothing filter-based intensity modulation: A spectral preserve image fusion technique for improving spatial details," *Int. J. Remote Sens.*, vol. 21, no. 18, pp. 3461–3472, 2000.
- [66] Stanislas de Béthune, Fabrice Muller, and Jean-Paul Donnay, "Fusion of multispectral and panchromatic images by local mean and variance matching filtering techniques," *Fusion of Earth Data*, pp. 28–30, 1998.
- [67] Ute G Gangkofner, Pushkar S Pradhan, and Derrold W Holcomb, "Optimizing the high-pass filter addition technique for image fusion," *Photogramm. Eng. Remote Sens.*, vol. 73, no. 9, pp. 1107–1118, 2007.
- [68] Alan R Gillespie, Anne B Kahle, and Richard E Walker, "Color enhancement of highly correlated images. ii. channel ratio and chromaticity transformation techniques," *Remote Sens. Environ.*, vol. 22, no. 3, pp. 343–365, 1987.
- [69] Chris Padwick, Michael Deskevich, Fabio Pacifici, and Scott Smallwood, "Worldview-2 pan-sharpening," in *Proceedings of the ASPRS 2010 Annual Conference, San Diego, CA, USA*, 2010, vol. 2630.
- [70] Te-Ming Tu, Ping Sheng Huang, Chung-Ling Hung, and Chien-Ping Chang, "A fast intensity-hue-saturation fusion technique with spectral adjustment for ikonos imagery," *IEEE Geosci. Remote Sens. Lett.*, vol. 1, no. 4, pp. 309–312, 2004.
- [71] Craig A Laben and Bernard V Brower, "Process for enhancing the spatial resolution of multispectral imagery using pan-sharpening," Jan. 4 2000, US Patent 6,011,875.
- [72] Andrea Garzelli, Filippo Nencini, and Luca Capobianco, "Optimal mmse pan sharpening of very high resolution multispectral images," *IEEE Trans. Geosci. Remote Sens.*, vol. 46, no. 1, pp. 228–236, 2007.
- [73] Dzmity Bahdanau, Kyunghyun Cho, and Yoshua Bengio, "Neural machine translation by jointly learning to align and translate," *arXiv preprint arXiv:1409.0473*, 2014.
- [74] Ashish Vaswani, Noam Shazeer, Niki Parmar, Jakob Uszkoreit, Llion Jones, Aidan N Gomez, Łukasz Kaiser, and Illia Polosukhin, "Attention is all you need," in *Proc. NIPS*, 2017, pp. 5998–6008.
- [75] Han Zhang, Ian Goodfellow, Dimitris Metaxas, and Augustus Odena, "Self-attention generative adversarial networks," *arXiv preprint arXiv:1805.08318*, 2018.

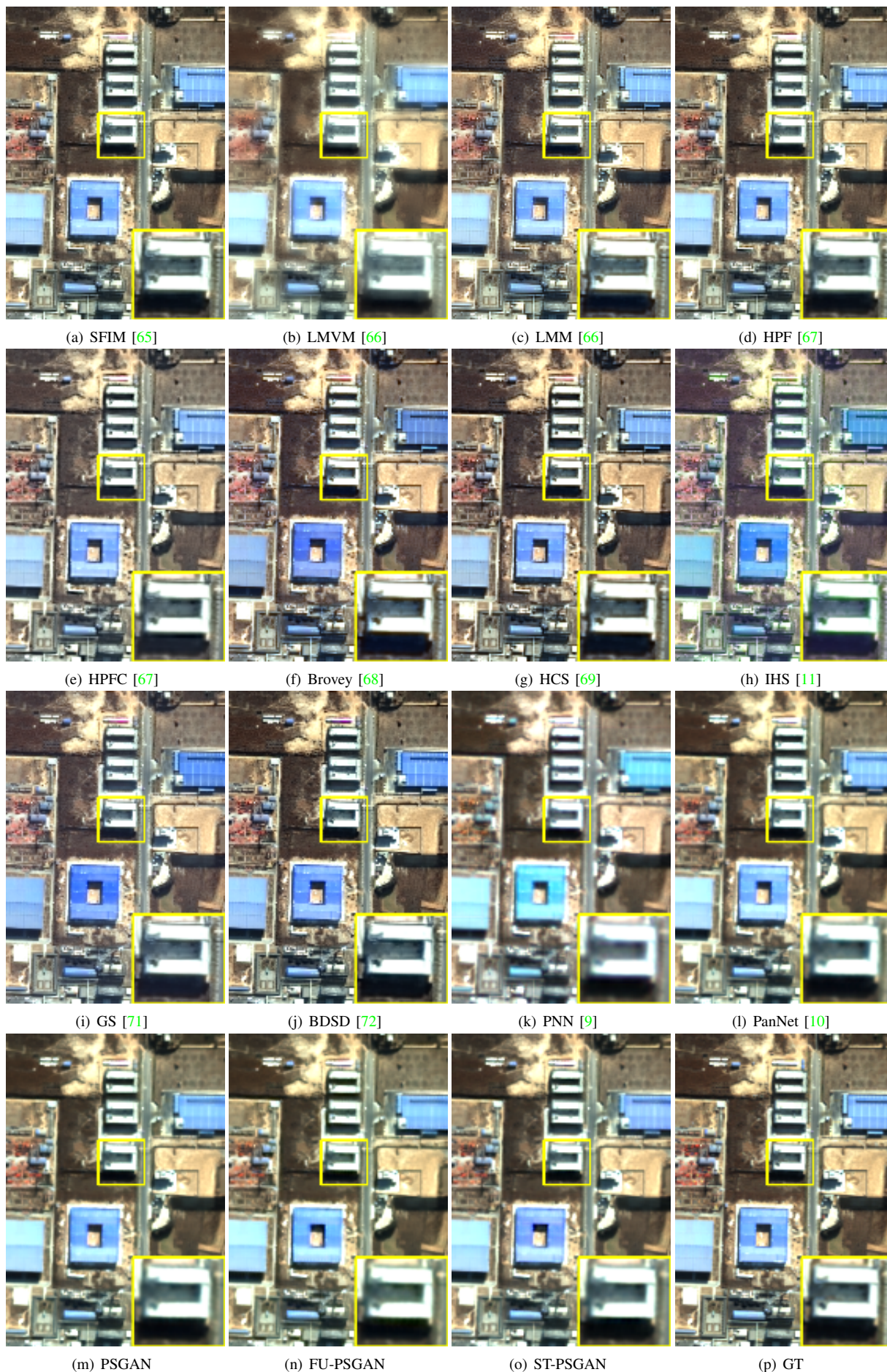


Fig. 5. Visual comparison on QB images. Images are displayed in RGB combination. All images have the same size of  $200 \times 140$  pixels.

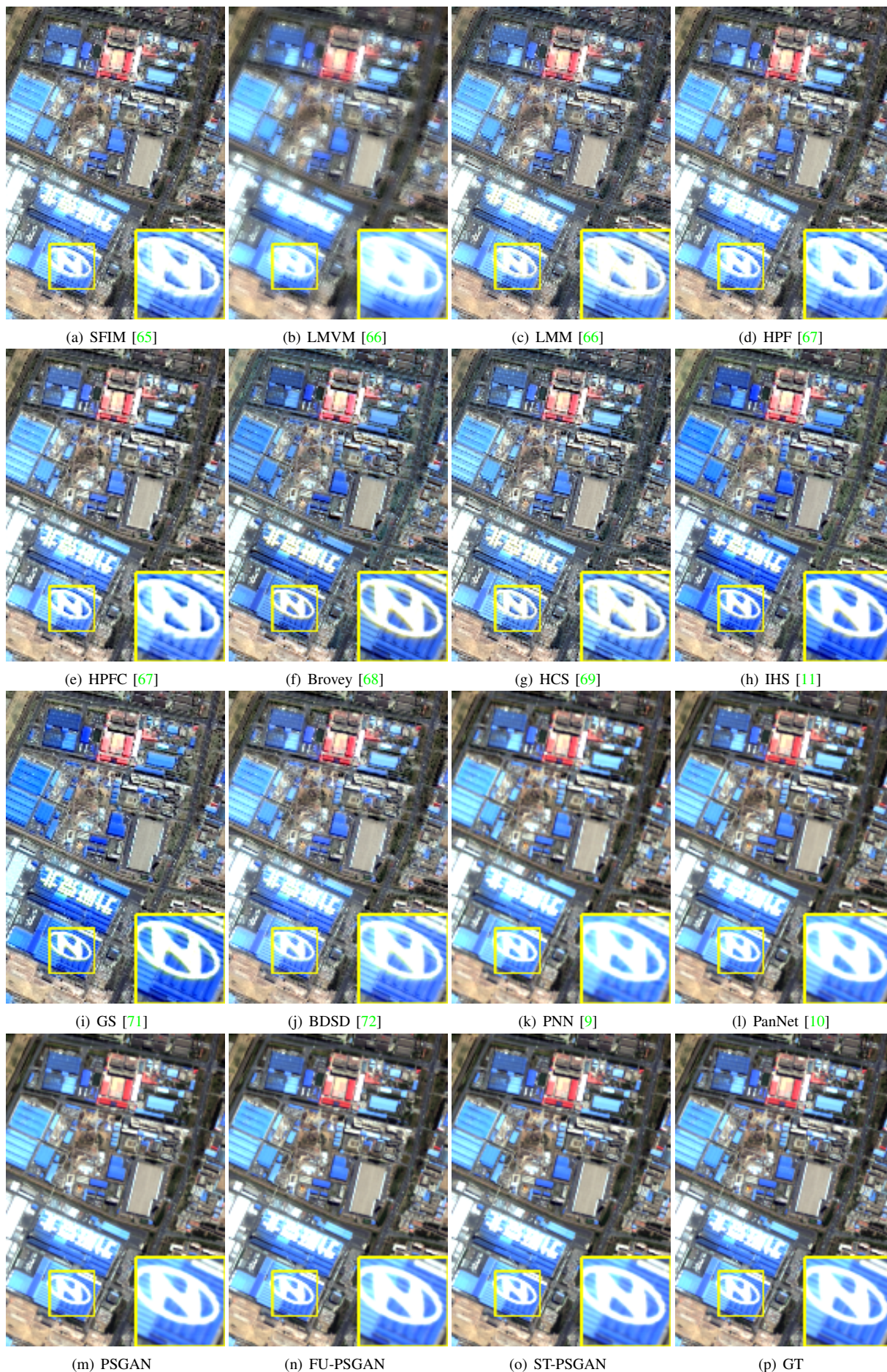


Fig. 6. Visual comparison on GF-2 images. Images are displayed in RGB combination. All images have the same size of  $200 \times 140$  pixels.